Tribology International 181 (2023) 108345

Contents lists available at ScienceDirect

Tribology International

journal homepage: www.elsevier.com/locate/triboint

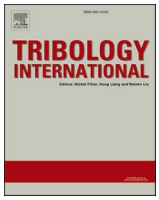

A linear non-Hertzian unsteady tangential wheel-rail contact model

Luis Baeza [a,*], Stefano Bruni [b], Juan Giner-Navarro [a], Binbin Liu [b]

[a] I2MB, Universitat Politècnica de València, Valencia, Spain
[b] Dipartimento di Meccanica, Politecnico di Milano, Milan, Italy

ARTICLE INFO

Keywords:
Wheel-rail contact
Non-Hertzian contact
Rolling contact
Linear contact
Rolling noise
Non-steady-state contact

ABSTRACT

The increase in computational capacity has considerably reduced the use of linear models for wheel/rail tangential contact, being currently replaced by theories that adopt non-linear formulations able to address the most complex conditions realistically. However, linear formulations are difficult to replace in certain applications such as acoustic problem modelling, in which case a linear formulation of the track-contact-vehicle system is needed. The vibration that appears in this type of problem covers a wide range of audible frequencies, so, in addition to linearity, these theories are required to be non-stationary. The literature in contact mechanics gives response to this problem through models that consider low creepage levels, but it remains to cover other conditions in which the mean creepage is not small, such as when a railway vehicle negotiates a curve.

This work presents a new theory of unsteady linear tangential rolling contact for non-Hertzian areas that considers kinematics as the sum of a constant creepage resulting from large stationary forces (such as those that occur when the vehicle negotiates a curve with constant radius) and small variable creepage due to a high-frequency phenomenon (e.g. the dynamic interaction between the vehicle and the track). The model is based on the Variational Theory (i.e. the CONTACT method for tangential problems), from which a linear formulation with variable creepage is deduced. According to this formulation, the non-steady state contact problem can be solved for any shape of the wheel/rail contact region, requiring a much smaller computational effort than the general unsteady CONTACT approach. The results show a satisfactory agreement of the proposed model to the unsteady CONTACT version, hence confirming the soundness of the proposed contact model.

1. Introduction

The wheel/rail contact pair is a crucial component of all railway systems, largely affecting railway vehicle dynamics and train/track interaction. The tractions in the contact patch and the resultant forces largely determine the overall dynamics of the system and typical damage phenomena such as wear, rolling contact fatigue, rail corrugation and wheel out-of-roundness [1].

Models of wheel/rail contact evolved remarkably over more than one century of research [2,3] so that a variety of modelling approaches are now available for different applications ranging from the simulation of non-linear vehicle dynamics in a relatively low frequency range (up to 20–30 Hz) to the study of train-track interaction effects in the high-frequency range (up to hundreds or even thousands of Hz) that are relevant to some damage phenomena and to rolling noise [4].

Most modelling approaches assume steady-state conditions in the contact patch: this means the frequency of time-varying contact parameters such as the normal force and the creepages is sufficiently low so that these quantities may be assumed to remain nearly constant while a material particle flows through the contact area. This assumption is justified by the fact that these dynamic variations are determined by the response of the vehicle to either deterministic or stochastic features of the track which all have wavelengths significantly longer than the width of the contact patch in longitudinal direction. However, when focusing on high-frequency train-track interaction, the dynamics of the system is determined by the roughness of the rolling surfaces having wavelengths in the same order of magnitude, or even shorter, than the contact patch size and in this case non-steady-state (NSS) effects become relevant and cannot be neglected. Furthermore, contact conditions implying the fast transition from one creepage regime to another, such as the sudden application of traction or braking forces, may require to be treated under NSS assumptions. The consideration of NSS effects implies a significant increase of the complexity of the problem because the contact region becomes a dynamic system in itself, whose dynamics must be described either in the time or frequency domain.

So far, only a limited number of attempts were made to model

* Correspondence to: Universidad Politécnica de Valencia, Camino de Vera, s/n, 46022 Valencia, Spain.
E-mail address: baeza@mcm.upv.es (L. Baeza).

https://doi.org/10.1016/j.triboint.2023.108345
Received 14 December 2022; Received in revised form 27 January 2023; Accepted 11 February 2023
Available online 13 February 2023

wheel/rail contact under NSS conditions. A first contribution was made by Kalker [5,6] who considered the transient situation arising when a traction force is suddenly applied to a wheel and kept constant in time. The results obtained show that the transition from the distribution of tangential stresses corresponding to a Cattaneo shift to that of steady-state rolling takes place over a very short distance travelled by the wheel, in the order of few times the longitudinal width of the contact region, thereby confirming the appropriateness of the steady-state assumption for most wheel/rail contact problems. The effect of NSS effects in a transient situation was took up again by Vollebregt [7] and the results he obtained show the presence of high-frequency and low-damped oscillations in the frictional contact force. These results are obtained however for a sphere rolling down an inclined plane and therefore neglect damping effects introduced in a railway vehicle by primary suspensions. The two above-cited references are the only ones addressing NSS conditions arising from transient dynamics of the vehicle. The other attempts to consider NSS wheel/rail contact forces consider excitation arising from corrugation and/or short-wavelength corrugation [8].

In terms of the modelling methods proposed for the NSS contact problem, one possible approach is to use Kalker's variational method [5,6]. This method, referred below as unsteady CONTACT, allows to consider non-Hertzian contact conditions [9] and the partitioning of the contact patch into adhesion and slip regions but is quite demanding from a computational point of view, despite the enhancements recently introduced by Vollebregt and co-workers [10,11]. An alternative approach is the extension to NSS conditions of Kalker's simplified theory known as FASTSIM. This was proposed initially by Shen and Li [12] for elliptic contacts using the same flexibility coefficients proposed by Kalker for the steady-state formulation of the linear theory, but the accuracy with respect to unsteady CONTACT is acceptable only for moderate creepage values. The NSS FASTSIM approach was extended by Alonso and Gimenez [13] and then by Guiral et al. [14], altering the definition of the flexibility coefficients to consider NSS conditions: in this way, the accuracy of the method is improved compared to the original implementation proposed by Shen and Li, but still non-negligible deviations from NSS CONTACT are found and the approach remains limited to Hertzian contact patches.

The above-mentioned approaches can consider arbitrary values of the creepages arising in the contact patch. If instead the time-varying component of the creepages is assumed to be small, the NSS contact problem can be formulated in terms of linear differential equations that can be solved in the frequency domain. This is the approach followed by Gross-Thebing and Knothe [15], resulting in a formulation in the frequency domain of the linear creepage-creep force relationship which makes use of frequency-dependent coefficients representing a generalization to the NSS case of the linear theory coefficients. This formulation is however confined to the case of an elliptic contact patch and assumes adhesion takes place over the entire contact region except an infinitesimally small strip at the trailing edge, whilst this latter assumption is removed in an extension of the method by Gross-Thebing [16].

The aim of this paper is to propose a numerical approach to treat the NSS tangential contact problem under the assumption of small time-varying creepage components, as done in references [15,16], but considering a generic contact patch shape as well as generic non-zero mean values for all creepage components. The developed mathematical expression associated with the proposed model is linear, which allows solving eigenproblems and carrying out analyses in the frequency domain. Consequently, this model opens up doors to addressing rolling noise problems when the vehicle is running on a curve. The resulting implementation, described in Section 2, is extremely efficient from the computational point of view, thus enabling the fast computation of contact forces and, at the same time, shows excellent accuracy with respect to the NSS CONTACT algorithm for a variety of cases, as reported in Section 3 of this paper.

2. Contact model

The contact model developed in this work is based on the CONTACT algorithm for tangential problems, which was published in Ref. [6]. The main hypotheses of CONTACT assume non-conformal contact [17], suppose that the solids behave elastically as infinite half-spaces and Coulomb's law is assumed with constant friction coefficient [6]. It is also supposed that the elastic behaviours of the wheel and the rail are the same, which implies that the normal tractions do not depend on the tangential ones. These basic assumptions are also adopted by the model developed in this paper.

A moving reference system $\mathbf{X}_1\mathbf{X}_2\mathbf{X}_3$ is chosen in the present work, whose origin is the centre of pressure associated with the normal traction distribution. The $\mathbf{X}_1$-axis corresponds to the rolling direction, the $\mathbf{X}_3$-axis is normal to the contact area (positive upwards), and the $\mathbf{X}_2$-axis is associated with the lateral direction, positive according to a right-handed frame of reference, as depicted in Fig. 1.

The original CONTACT method performs a discretisation of the potential contact area through a regular mesh with $2a \times 2b$ rectangular elements. In the elements belonging to the contact area, the normal and tangential tractions are assumed to be constant. Let's p_τ^e be the tangential constant traction of the e-th element of the mesh, according to the τ direction (where subindex τ is 1 or 2, here and beyond). The tractions p_τ^e are included in a vector of tangential tractions $\mathbf{p}$. Without loss of generality, vector $\mathbf{p}$ is sorted as follows

$$\mathbf{p} = \left\{ p_1^1 \quad p_2^1 \quad p_1^2 \quad p_2^2 \quad \cdots \quad p_1^N \quad p_2^N \right\}^{\mathrm{T}}, \tag{1}$$

N being the number of elements in the contact area. In this work, p_τ^e refers the tractions applied in the wheel contact area (the tractions on the rail have the same magnitude but opposite directions).

The CONTACT model adopts a classical kinematic formulation within Continuum Mechanics that combines the velocities associated with the rigid configuration of the solids with the velocities corresponding to the deformed configuration (these latter being calculated by means of finite differences). Following a collocation method, the kinematics equations on the contact surface must be satisfied at a point of each element belonging to the contact area. Next, constitutive relations allow formulating the collocation point displacements associated with the deformed configuration of the solids as a function of the tractions in each element. This gives rise to the fundamental equation of the CONTACT method, which is

$$\mathbf{s} = \mathbf{w} + \frac{1}{\Delta t}(\mathbf{A}\mathbf{p} - \mathbf{A}_0\mathbf{p}_0), \tag{2}$$

where vectors $\mathbf{s}$ and $\mathbf{w}$ contain the slip velocities and the tangential rigid body velocities of the collocation points at the current instant t; $\mathbf{p}_0$ is the tangential traction vector at the previous instant t_0; matrix $\mathbf{A}$ is the elastic coefficient matrix that relates the current tangential traction vector $\mathbf{p}$ with the displacements of the collocation points at the current instant; matrix $\mathbf{A}_0$ is the elastic coefficient matrix that relates the

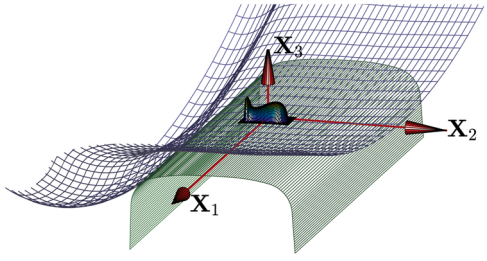

Fig. 1. Frame of reference $\mathbf{X}_1\mathbf{X}_2\mathbf{X}_3$ centred at the centre of pressure between the rail (lower body) and the wheel (upper one). The figure also shows the wheel (S1002 profile) and the rail (UIC60) surfaces, and the corresponding normal traction distribution.

tangential tractions that are applied in the elements of the previous instant mesh with the displacements of the collocation points at the current instant; and Δt is the time step (that is $\Delta t = t - t_0$). A complete explanation of Eq. (2) development (which includes the elastic coefficient formulae) can be found in Ref. [6]. The integration of Eq. (2) allows calculating the non-stationary contact process for non-Hertzian areas.

If the contact traction distribution $\mathbf{p}$ at instant t is equal to the tractions $\mathbf{p}_0$ at the previous instant t_0, then the steady-state conditions are reached. Imposing $\mathbf{p} = \mathbf{p}_0$ on Eq. (2), the fundamental equation of CONTACT for the tangential steady-state contact problem is obtained, which is

$$\overline{\mathbf{s}} = \overline{\mathbf{w}} + \frac{1}{\Delta t}(\mathbf{A} - \mathbf{A}_0)\overline{\mathbf{p}}, \tag{3}$$

$\overline{\mathbf{s}}$, $\overline{\mathbf{w}}$ and $\overline{\mathbf{p}}$ being the corresponding parameters of the steady-state contact problem. The solutions of Eqs. (2) and (3) are carried out through Kalker's TANG algorithm and Newton iteration (an iterative process in which systems of equations are solved from successive hypotheses about if the elements belong to the adhesion or the slip area). A complete description of the unsteady and the steady-state CONTACT methods can be found in Kalker's monograph [6].

Let's assume that any contact parameter can be formulated as the sum of a constant and a variable value. For example, for the case of the velocity vector associated with the rigid body configuration, this formulation would be

$$\mathbf{w}(t) = \overline{\mathbf{w}} + \widetilde{\mathbf{w}}(t), \tag{4}$$

where $\overline{\mathbf{w}}$ is the mean or steady value, and $\widetilde{\mathbf{w}}(t)$ the parameter variation. This decomposition is also adopted for $\mathbf{s}$ and $\mathbf{p}$. When this approach is implemented in the general CONTACT formula in Eq. (2), the following equation is found

$$\overline{\mathbf{s}} + \widetilde{\mathbf{s}}(t) = \overline{\mathbf{w}} + \widetilde{\mathbf{w}}(t) + \frac{1}{\Delta t}\mathbf{A}\overline{\mathbf{p}} + \frac{1}{\Delta t}\mathbf{A}\widetilde{\mathbf{p}}(t) - \frac{1}{\Delta t}\mathbf{A}_0\overline{\mathbf{p}} - \frac{1}{\Delta t}\mathbf{A}_0\widetilde{\mathbf{p}}(t_0). \tag{5}$$

Combining the last expression with Eq. (3), the constant terms vanish, obtaining

$$\widetilde{\mathbf{s}}(t) = \widetilde{\mathbf{w}}(t) + \frac{1}{\Delta t}\mathbf{A}\widetilde{\mathbf{p}}(t) - \frac{1}{\Delta t}\mathbf{A}_0\widetilde{\mathbf{p}}(t_0). \tag{6}$$

If the variation of the contact parameters is small, the elements belonging to the slip and to the adhesion areas are known a priori. Since the harmonic variations are small, the slip and the adhesion areas are the same as the steady-state problem. Consequently, the local slip velocity variation $\widetilde{s}_\tau^e$ of the elements at the adhesion area is zero.

Let's define $\mathbf{p}^e(t)$ as the traction in the e-th element of the mesh, belonging this element to the slip area. The current traction $\mathbf{p}^e(t)$ and the mean traction $\overline{\mathbf{p}}^e$ have the same modulus (which is the friction coefficient times the normal traction) and they form an angle β as can be seen in Fig. 2. Assuming that the variation parameters are small, the traction variation $\widetilde{\mathbf{p}}^e$ and the mean traction $\overline{\mathbf{p}}^e$ are orthogonal, hence

$$\widetilde{\mathbf{p}}^e \approx \sin\beta \begin{Bmatrix} -\overline{p}_2^e \\ \overline{p}_1^e \end{Bmatrix} \text{if} e \in \textit{sliparea}. \tag{7}$$

Since the element is located at the slip area, the local slip velocity $\mathbf{s}^e$ and the traction $\mathbf{p}^e$ are aligned but with opposite directions, so the angle between $\mathbf{s}^e$ and $\overline{\mathbf{s}}^e$ is β. Through the cross product of $\mathbf{s}^e$ and $\overline{\mathbf{s}}^e$, the following relation is obtained

$$\overline{\mathbf{s}}^e \times \mathbf{s}^e = \overline{\mathbf{s}}^e \times (\overline{\mathbf{s}}^e + \widetilde{\mathbf{s}}^e) = (\overline{s}_1^e \widetilde{s}_2^e - \overline{s}_2^e \widetilde{s}_1^e)\mathbf{x}_3 = |\overline{\mathbf{s}}^e||\mathbf{s}^e|\sin\beta\mathbf{x}_3, \tag{8}$$

$\mathbf{x}_3$ being a unit vector in the $\mathbf{X}_3$ direction. From Eqs. (7) and (8), and assuming that $|\overline{\mathbf{s}}^e| \approx |\mathbf{s}^e|$, the traction variation at the element that belongs to the slip area can be formulated as follows

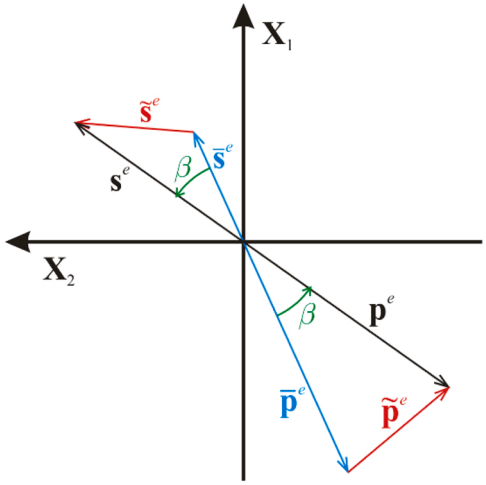

Fig. 2. Sketch of the tangential traction and the local slip velocity associated with an element at the slip area.

$$\widetilde{\mathbf{p}}^e \approx \frac{1}{|\overline{\mathbf{s}}^e|^2}\begin{pmatrix} \overline{p}_2^e\overline{s}_2^e & -\overline{p}_2^e\overline{s}_1^e \\ -\overline{p}_1^e\overline{s}_2^e & \overline{p}_1^e\overline{s}_1^e \end{pmatrix}\widetilde{\mathbf{s}}^e \quad \text{if } e \in \text{slip area}. \tag{9}$$

If the first order Maclaurin approximation of the variable traction is performed instead of carrying out the previous geometric simplifications (regarding Eq. (7) and $|\overline{\mathbf{s}}^e| \approx |\mathbf{s}^e|$), the formula in Eq. (9) is identically obtained.

If the last development is assumed, then Eq. (6) is linear. If harmonic variation of the contact parameters is considered, Eq. (6) becomes

$$\widetilde{\mathbf{S}}e^{i\omega t} = \widetilde{\mathbf{W}}e^{i\omega t} + \Delta t^{-1}\mathbf{A}\widetilde{\mathbf{P}}e^{i\omega t} - \Delta t^{-1}\mathbf{A}_0\widetilde{\mathbf{P}}e^{i\omega t_0}, \tag{10}$$

and consequently

$$\widetilde{\mathbf{S}} = \widetilde{\mathbf{W}} + \Delta t^{-1}\left(\mathbf{A} - \mathbf{A}_0 e^{-i\omega\Delta t}\right)\widetilde{\mathbf{P}}, \tag{11}$$

$\widetilde{\mathbf{S}}$, $\widetilde{\mathbf{W}}$ and $\widetilde{\mathbf{P}}$ being the complex coefficients defining the harmonic variation of the contact parameters, ω the variation frequency, Δt the time increment ($\Delta t = t - t_0$), and i the imaginary unit. The unknows of Eq. (11) are the tractions of the elements in the adhesion area, and the local slip velocities of the elements in the slip area. These variables are included in a vector of unknows $\widetilde{\mathbf{Q}}$, with dimension $2N$. From Eq. (9), it is possible to obtain matrices $\mathbf{B}$ and $\mathbf{C}$, such as

$$\widetilde{\mathbf{P}} = \mathbf{B}\widetilde{\mathbf{Q}}, \tag{12}$$

$$\widetilde{\mathbf{S}} = \mathbf{C}\widetilde{\mathbf{Q}}. \tag{13}$$

Note that $\mathbf{C}$ is a topological matrix formed by ones and zeros, whereas matrix $\mathbf{B}$ is assembled with the elementary matrix in Eq. (9), ones and zeros.

If Eqs. (12) and (13) are substituted in Eq. (11), $\widetilde{\mathbf{Q}}$ can be calculated through the following formula

$$\widetilde{\mathbf{Q}} = \left[\mathbf{C} + \Delta t^{-1}\left(\mathbf{A} - \mathbf{A}_0 e^{-i\omega\Delta t}\right)\mathbf{B}\right]^{-1}\widetilde{\mathbf{W}}. \tag{14}$$

In order to calculate the creep coefficients, it is convenient to define the following vectors

$$\mathbf{U}_1 = \{1 \quad 0 \quad 1 \quad 0 \quad \ldots \quad 1 \quad 0\}^{\mathrm{T}}, \tag{15}$$

$$\mathbf{U}_2 = \{0 \quad 1 \quad 0 \quad 1 \quad \ldots \quad 0 \quad 1\}^{\mathrm{T}}, \tag{16}$$

$$\mathbf{U}_{sp} = \left\{-x_2^1 \quad x_1^1 \quad -x_2^2 \quad x_1^2 \quad \ldots \quad -x_2^N \quad x_1^N\right\}^{\mathrm{T}}, \tag{17}$$

where x_τ^e is the coordinate in the τ-direction of the collocation point

associated with the e-th element of the mesh, and N is the number of elements in the mesh. The dimension of these three vectors is $2N$. In accordance with the vector arrangement in Eq. (1), the amplitudes of the total force variation in the longitudinal $\widetilde{F}_1$ and the lateral $\widetilde{F}_2$ direction can be expressed as follows

$$\widetilde{F}_\tau = 4ab\mathbf{U}_\tau^{\mathrm{T}}\widetilde{\mathbf{P}}, \tag{18}$$

where a and b are the half-width of the elements in the rolling and lateral directions, respectively. Analogously, the amplitude of the spin moment is calculated as follows

$$\widetilde{M}_{sp} = 4ab\mathbf{U}_{sp}^{\mathrm{T}}\widetilde{\mathbf{P}}. \tag{19}$$

The amplitude of the tangential rigid body velocities in elements of the adhesion area $\widetilde{\mathbf{W}}$ can be calculated from the longitudinal $\widetilde{\xi}_1$, lateral $\widetilde{\xi}_2$ and spin $\widetilde{\xi}_{sp}$ creepage variations through the following formula

$$\widetilde{\mathbf{W}} = \widetilde{\xi}_1 V\,\mathbf{U}_1 + \widetilde{\xi}_2 V\,\mathbf{U}_2 + \widetilde{\xi}_{sp} V\,\mathbf{U}_{sp}, \tag{20}$$

V being the wheel speed. Eq. (20) derives from the kinematic relationship

$$\begin{bmatrix} w_1^e \\ w_2^e \end{bmatrix} = V \begin{bmatrix} \xi_1 - \xi_{sp}\, x_2^e \\ \xi_2 + \xi_{sp}\, x_1^e \end{bmatrix} \tag{21}$$

applied to all collocation points in the discretised contact patch. The above equation is the classic expression that relates the velocities of two points fixed on a rigid body, combined with the definition of linear/spin creepage components (see further information in Ref. [18]).

From Eqs. (12), (14) and (20), the amplitude of the tangential traction variation is

$$\widetilde{\mathbf{P}} = V\mathbf{B}\left[\mathbf{C} + \Delta t^{-1}\left(\mathbf{A} - \mathbf{A}_0 \mathrm{e}^{-\mathrm{i}\omega\Delta t}\right)\mathbf{B}\right]^{-1}\left(\widetilde{\xi}_1\mathbf{U}_1 + \widetilde{\xi}_2\mathbf{U}_2 + \widetilde{\xi}_{sp}\mathbf{U}_{sp}\right), \tag{22}$$

or by means of the compact form

$$\widetilde{\mathbf{P}} = \frac{1}{4ab}\mathbf{D}\left(\widetilde{\xi}_1\mathbf{U}_1 + \widetilde{\xi}_2\mathbf{U}_2 + \widetilde{\xi}_{sp}\mathbf{U}_{sp}\right), \tag{23}$$

where

$$\mathbf{D} = 4abV\mathbf{B}\left[\mathbf{C} + \Delta t^{-1}\left(\mathbf{A} - \mathbf{A}_0 \mathrm{e}^{-\mathrm{i}\omega\Delta t}\right)\mathbf{B}\right]^{-1}. \tag{24}$$

By substituting Eq. (23) in Eqs. (18) and (19), the amplitudes of the total force/moment variation are formulated as follows

$$\widetilde{F}_1 = \mathbf{U}_1^{\mathrm{T}}\mathbf{D}\mathbf{U}_1\widetilde{\xi}_1 + \mathbf{U}_1^{\mathrm{T}}\mathbf{D}\mathbf{U}_2\widetilde{\xi}_2 + \mathbf{U}_1^{\mathrm{T}}\mathbf{D}\mathbf{U}_{sp}\widetilde{\xi}_{sp}, \tag{25}$$

$$\widetilde{F}_2 = \mathbf{U}_2^{\mathrm{T}}\mathbf{D}\mathbf{U}_1\widetilde{\xi}_1 + \mathbf{U}_2^{\mathrm{T}}\mathbf{D}\mathbf{U}_2\widetilde{\xi}_2 + \mathbf{U}_2^{\mathrm{T}}\mathbf{D}\mathbf{U}_{sp}\widetilde{\xi}_{sp}, \tag{26}$$

$$\widetilde{M}_{sp} = \mathbf{U}_{sp}^{\mathrm{T}}\mathbf{D}\mathbf{U}_1\widetilde{\xi}_1 + \mathbf{U}_{sp}^{\mathrm{T}}\mathbf{D}\mathbf{U}_2\widetilde{\xi}_2 + \mathbf{U}_{sp}^{\mathrm{T}}\mathbf{D}\mathbf{U}_{sp}\widetilde{\xi}_{sp}. \tag{27}$$

By adapting Kalker's Linear Theory notation, the force variation amplitudes are

$$\widetilde{F}_1 = -f_{11}\widetilde{\xi}_1 - f_{12}\widetilde{\xi}_2 - f_{13}\widetilde{\xi}_{sp}, \tag{28}$$

$$\widetilde{F}_2 = -f_{21}\widetilde{\xi}_1 - f_{22}\widetilde{\xi}_2 - f_{23}\widetilde{\xi}_{sp}, \tag{29}$$

$$\widetilde{M}_{sp} = -f_{31}\widetilde{\xi}_1 - f_{32}\widetilde{\xi}_2 - f_{33}\widetilde{\xi}_{sp}, \tag{30}$$

where f_{jk} are the creep coefficients. It must be pointed out that the creep coefficients f_{jk} are complex values that depend on the creepage variation frequency ω and the parameters associated with the steady-state contact problem.

3. Results

The results in this section are intended to estimate the proposed model's accuracy and analyse the characteristic of the solution provided through the creep coefficients. Comparisons are provided with the unsteady version of CONTACT for tangential problems, used as a reference solution.

For most of the results, the calculation conditions correspond to a wheelset with GV40 wheel profiles on a track with standard gauge (1435 mm) and UIC60 rails with 1:40 inclination. The wheelset is centred on the track, and the load per wheel is 10 tons. In this case, the Hertzian contact conditions are satisfied, and the contact area is an ellipse, being the semiaxes in the longitudinal and lateral directions 7.18 and 5.29 mm, respectively. Sections 3.1 to 3.3 present calculations for this contact area considering different assumptions regarding the creepage. Section 3.4 analyses the properties of the creep coefficients calculated through this model. Section 3.5 performs an example of calculation for a non-Hertzian area (a wheel profile S1002 is adopted). The vehicle speed at which the calculations are carried out is 50 km/h in all cases.

3.1. Response to longitudinal creepage harmonic variation

In the present section, the longitudinal creepage is formulated as the sum of a mean value and a harmonic variation, that is,

$$\xi_1(t) = \overline{\xi}_1 + \widetilde{\xi}_1 \cos\omega t. \tag{31}$$

The mean value for the first calculation is $\overline{\xi}_1 = 0.001$, the variable amplitude $\widetilde{\xi}_1 = 5{\cdot}10^{-5}$ and the frequency $\omega = 1$ kHz. The lateral creepage and the spin are null. The steady-state solution of the contact problem for the creepage mean value $\overline{\xi}_1$ is obtained through Eq. (3).

The creep coefficients computed in this case are shown in Table 1. Owing to the symmetry of the contact patch, only coefficients f_{11}, f_{22}, f_{23} and f_{32} are significant, so F_2 and M_{sp} can be neglected in this study. Fig. 3 presents the longitudinal force response $F_1(t)$ calculated through the integration of Eq. (2) when the initial conditions are null (unsteady CONTACT), by means of successive solutions of Eq. (3) (steady-state CONTACT), and through the proposed model. It can be seen that the stationary model differs considerably from the reference one, in modulus and phase, and cannot be considered suitable for the present calculation conditions. Consequently, this result invalidates any other steady-state model, at least for the present calculation conditions. On the other hand, the responses calculated through the reference model (unsteady CONTACT) and the proposed model are indistinguishable after a short transient associated with the initial conditions that are imposed in CONTACT. After the transient, the error of the proposed model with regard to the reference one is smaller than 1 Newton.

3.2. Response to generic harmonic creepage variation

In this section, a more complex kinematic case is considered: longitudinal, lateral and spin creepages occur simultaneously. The mean creepages are $\overline{\xi}_1 = \overline{\xi}_2 = 0.001$ and $\overline{\xi}_{sp} = -0.053$ rad/m. The variable creepages are taken as 5% of the corresponding mean values, i.e. $\widetilde{\xi}_1 =$

Table 1
Creep coefficients for $\omega = 1$ kHz, $\overline{\xi}_1 = 0.001$ and $\overline{\xi}_2 = \overline{\xi}_{sp} = 0$. The coefficients are expressed in SI units.

$f_{11} = 3.30{\cdot}10^5 - \mathrm{i}2.31{\cdot}10^6$	$f_{12} = 0.1 - \mathrm{i}0.1$	$f_{13} = 550.0 - \mathrm{i}2982.5$
$f_{21} = 0.6 - \mathrm{i}2.0$	$f_{22} = 3.32{\cdot}10^5 - \mathrm{i}2.53{\cdot}10^6$	$f_{23} = 2462.2 - \mathrm{i}1909.1$
$f_{31} = 418.2 - \mathrm{i}2438.0$	$f_{32} = -9425.7 - \mathrm{i}1.88{\cdot}10^4$	$f_{33} = 543.9 - \mathrm{i}863.1$

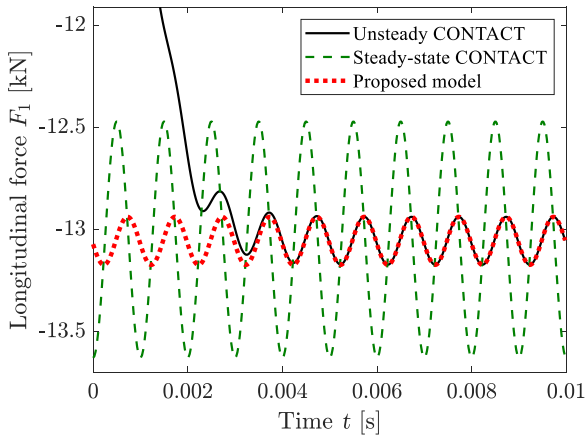

Fig. 3. Longitudinal forces calculated through the unsteady model, the steady-state contact model, and the proposed model when $\xi_1(t) = 10^{-3} + 5{\cdot}10^{-5}\cos(2\pi 1000t)$ and $\xi_2 = \xi_{sp} = 0$.

$\widetilde{\xi}_2 = 5{\cdot}10^{-5}$, and $\widetilde{\xi}_{sp} = 0.0027$ rad/m. The rest of the calculation conditions are the same as those of the previous section. The steady-state tangential traction distribution calculated for the mean creepages is plotted in Fig. 4.

Fig. 5 compares the forces calculated by means of the proposed model, and through integration of Eq. (2) when the initial conditions are null (unsteady CONTACT as reference). Fig. 5(a), (b) and (c) represent the longitudinal and lateral forces and the spin moment, respectively. The errors in the calculation of the forces by means of the proposed model are small compared with the reference, with deviations not exceeding 9.4 N for the longitudinal force, and 1 N for the lateral one (the amplitudes of the force variation in the longitudinal and lateral directions are 117 and 121 N, respectively). However, the relative errors are higher when computing the spin moment, but in this case the moment values are very small and would have a negligible influence on vehicle dynamics.

3.3. Response to pseudo-random creepage variation

In the two previous sections, longitudinal, lateral and spin creepages have been assumed to be in phase, and a harmonic waveform was assumed for creepage variation. In this section, the accuracy of the developed contact model will be assessed independently of the frequency and the phase between the three creepage components. To this end, it is considered that the creepages vary according to a finite-bandwidth white-noise signal approached through the following function

$$\xi_j(t) = \overline{\xi}_j + \widetilde{\xi}_j \sum_{n=0}^{N_h} \cos\left(\omega_n t + \alpha_{jn}\right), \tag{32}$$

where α_{jn} expresses a set of N_h random phases for each creepage direction j. The current calculation considers $N_h = 1000$ uniformly distributed frequencies ω_n, between 100 Hz and 5 kHz. The harmonic amplitudes are $\widetilde{\xi}_j = 10^{-6}$ for longitudinal and lateral creepages, and $\widetilde{\xi}_{sp} = 5{\cdot}10^{-6}$ rad/m for the spin. The peak to peak amplitudes of the creepage realisations are $1.34{\cdot}10^{-4}$ for the longitudinal creepage, $1.38{\cdot}10^{-4}$ for the lateral creepage and $7.61{\cdot}10^{-4}$ rad/m for the spin, whereas the standard deviations are $2.29{\cdot}10^{-5}$ for the longitudinal creepage, $2.25{\cdot}10^{-5}$ for the lateral creepage and $1.12{\cdot}10^{-4}$ rad/m for the spin. The rest of the parameters are identical to those selected in Section 3.2.

Fig. 6 compares the responses obtained through the reference model (unsteady CONTACT) and the proposed one. The initial conditions for the calculation with unsteady CONTACT correspond to those obtained through the steady-state CONTACT. The force values are calculated using the proposed model through the following formulation

$$F_1 = \overline{F}_1 - \Re\left(\sum_{n=1}^{N_h}\left[f_{11}\widetilde{\xi}_1 e^{i\alpha_{1n}} + f_{12}\widetilde{\xi}_2 e^{i\alpha_{2n}} + f_{13}\widetilde{\xi}_{sp} e^{i\alpha_{3n}}\right] e^{i\omega_n t}\right), \tag{33}$$

$$F_2 = \overline{F}_2 - \Re\left(\sum_{n=1}^{N_h}\left[f_{21}\widetilde{\xi}_1 e^{i\alpha_{1n}} + f_{22}\widetilde{\xi}_2 e^{i\alpha_{2n}} + f_{23}\widetilde{\xi}_{sp} e^{i\alpha_{3n}}\right] e^{i\omega_n t}\right), \tag{34}$$

where $\Re(\cdot)$ denotes the real part. The dependence of the creep coefficients on frequency has been omitted in the last equation, but it should be noted that $f_{ij} = f_{ij}(\omega_n)$.

Although the temporal response allows to appreciate a reasonable adjustment of the proposed model to the reference one, the information related to the ability of the new model for its implementation in linear models of vehicle/track system (such as those used in the calculation of rolling noise) can be better analysed in the frequency domain. Fig. 7 presents the Fourier transforms of the temporal signals shown in Fig. 6. A satisfactory agreement between the two models can be observed, especially in the medium and high frequency range. It should be noted that the differences appearing in some dips have little influence on the final response, since the ordinate axis is in logarithmic scale.

The main weakness of the new model would be associated with the simplifying hypotheses that were adopted. In this line, the effect of linearising the traction formula of the elements located at the slip area through the expression in Eq. (9) should be analysed. The more elements there are in the sliding area, the more tractions of these elements will be calculated through Eq. (9), and the impact of the linearisation on the accuracy of the proposed method could be more important. In order to assess this effect, the following calculation is carried out with larger mean creepages, i.e. $\overline{\xi}_1 = \overline{\xi}_2 = 0.0025$ and $\overline{\xi}_{sp} = -0.1$ rad/m. Fig. 8 shows the contact traction distribution, distinguishing both adhesion and slip areas. Fig. 9 plots the spectrum of the contact forces for these new calculation conditions, obtained from the response provided by CONTACT and the proposed model. It can be seen that the agreement is generally good except at low frequencies for the response corresponding to the longitudinal force F_1.

The simplifying hypothesis studied next is the assumption that the areas of adhesion and slip do not change during the unsteady contact process. To analyse the robustness of the model, a higher creepage variation is considered through the formula in Eq. (32). The creepage values are $\overline{\xi}_1 = \overline{\xi}_2 = 0.001$, $\overline{\xi}_{sp} = -0.053$ rad/m, $\widetilde{\xi}_1 = \widetilde{\xi}_2 = 10^{-5}$ and $\widetilde{\xi}_{sp} = 5{\cdot}10^{-5}$ rad/m, and the creepage variation coincides with the one of the previous calculation. It can be seen that the amplitude of the variable component reaches 75% of the mean creepage. The spectra of the

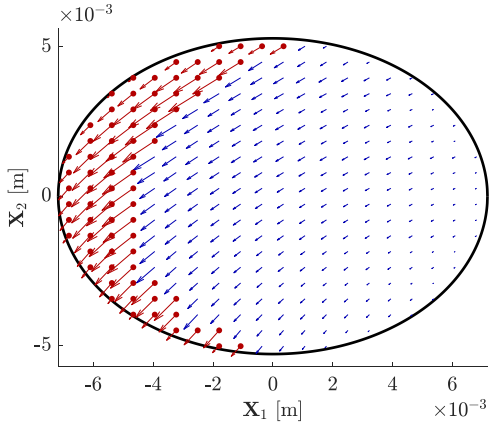

Fig. 4. Tangential traction distribution calculated through the steady-state contact model for $\overline{\xi}_1 = \overline{\xi}_2 = 0.001$ and $\overline{\xi}_{sp} = -0.053$ rad/m. Blue arrows are in the adhesion area whereas the slip area plots red arrows and dots.

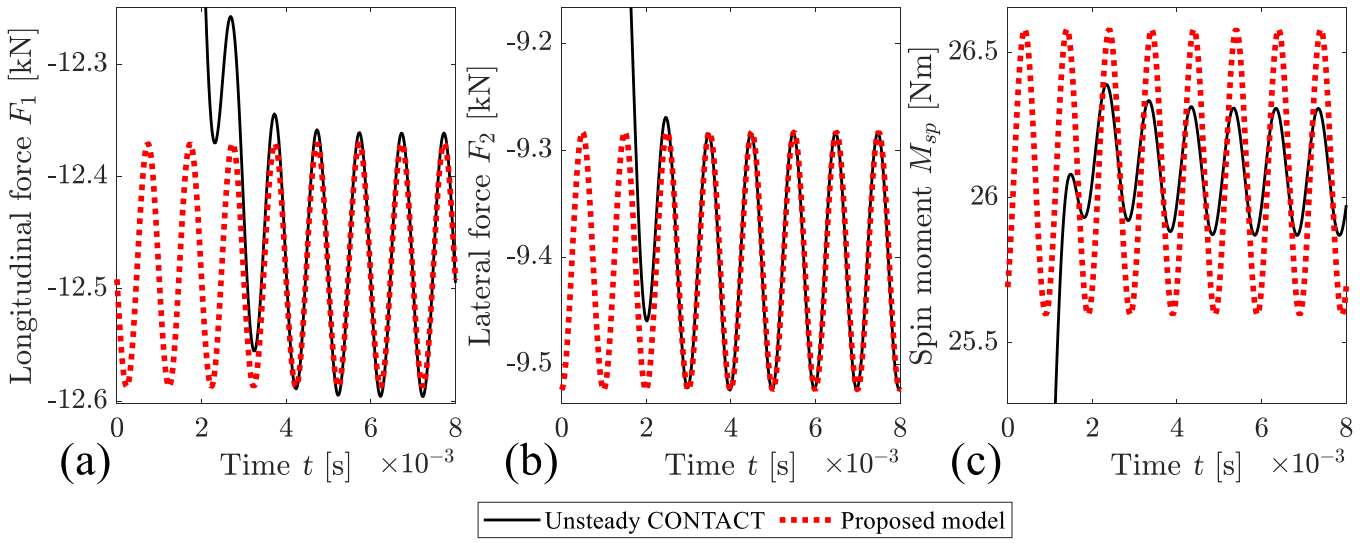

Fig. 5. Contact forces calculated through the unsteady CONTACT program and the proposed model when $\bar{\xi}_1 = \bar{\xi}_2 = 0.001$, $\bar{\xi}_{sp} = -0.053$ rad/m, $\tilde{\xi}_1 = \tilde{\xi}_2 = 5{\cdot}10^{-5}$, and $\tilde{\xi}_{sp} = 0.0027$ rad/m: (a) longitudinal contact force; (b) lateral contact force; (c) spin moment.

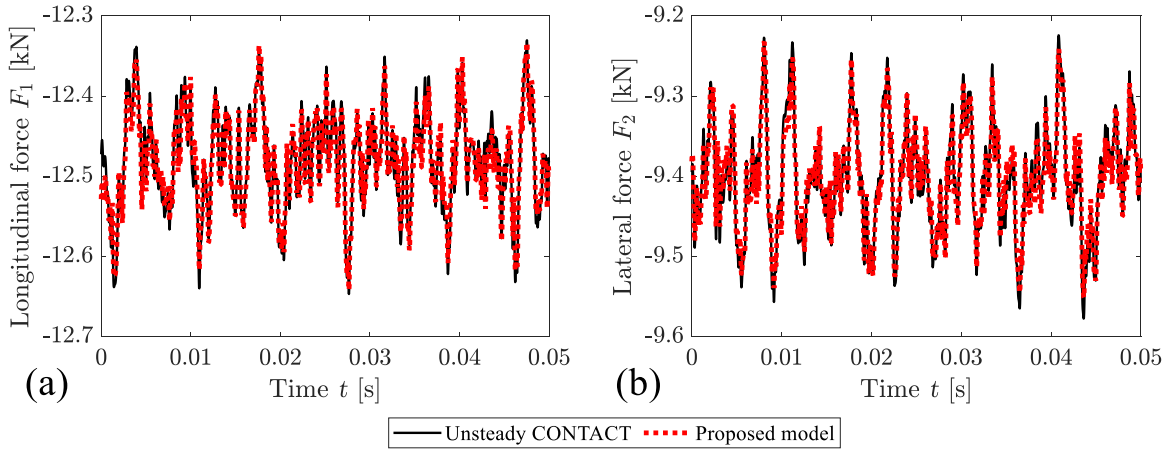

Fig. 6. Contact force responses to a pseudo-random creepage variation when $\bar{\xi}_1 = \bar{\xi}_2 = 0.001$, $\bar{\xi}_{sp} = -0.053$ rad/m, $\tilde{\xi}_1 = \tilde{\xi}_2 = 10^{-6}$ and $\tilde{\xi}_{sp} = 5{\cdot}10^{-6}$ rad/m. Comparison between the results obtained by the unsteady CONTACT and those from the proposed model: (a) longitudinal force; (b) lateral force.

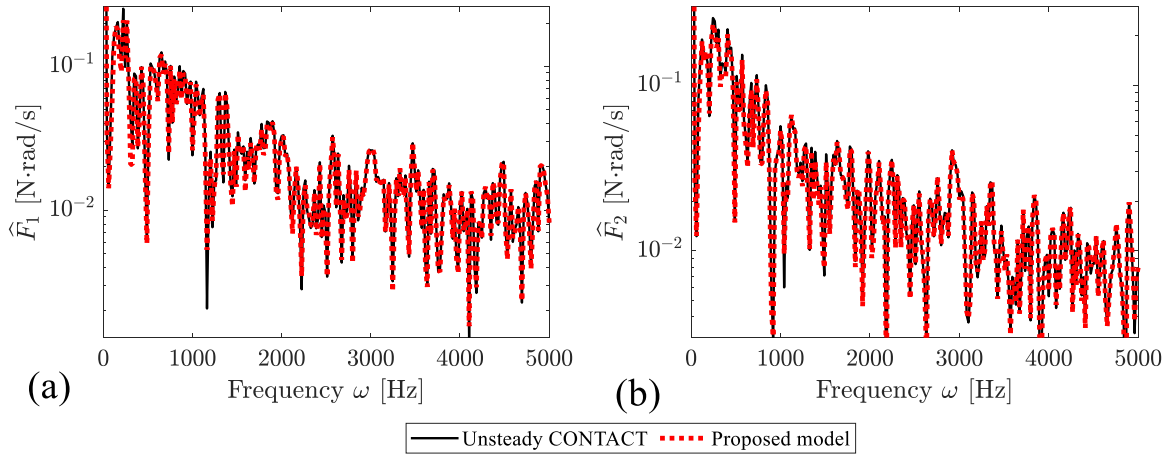

Fig. 7. Fourier transform of the contact forces presented in Fig. 6. Comparison between the results obtained by the unsteady CONTACT and those from the proposed model: (a) longitudinal force; (b) lateral force.

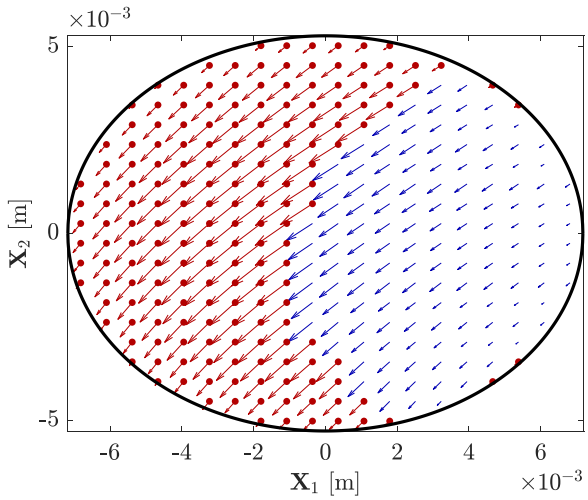

Fig. 8. Tangential traction distribution calculated through the steady-state CONTACT for $\bar{\xi}_1 = \bar{\xi}_2 = 0.0025$ and $\bar{\xi}_{sp} = -0.1$ rad/m. Blue arrows are in the adhesion area whereas the slip area plots red arrows and dots.

contact forces are shown in Fig. 10. It is worth noting that there is a good agreement between the results of the two models despite the significant level of creepage variation.

3.4. Creepage coefficients

Fig. 11 shows the longitudinal f_{11} and lateral f_{22} creep coefficients calculated as a function of the creepage variation frequency ω when the mean creepages are $\bar{\xi}_1 = \bar{\xi}_2 = 0.001$ and $\bar{\xi}_{sp} = -0.053$ rad/m. Fig. 11(a) presents the module of the creep coefficients, and Fig. 11(b) plots the argument. At low frequency, the values of f_{11} are much larger than f_{22}, being both real (their arguments are null and therefore, there is no phase difference between the contact forces and the creepages). Since creepage is proportional to the velocity of the wheel contact point, contact behaves as a damper when creepage varies at low-frequency. As the frequency increases, the damping capacity of the contact decreases because the creepage modulus becomes smaller, and its argument approaches $-90°$. If there is $90°$ delay of the force, the contact behaves not as a damper but as a stiffness. This result seems to indicate that when the creepage varies at high frequency, the wheel speed and, therefore, the rolling contact phenomena are negligible (the creepage varies but the wheel hardly rotates). Consequently, the contact behaves like a spring whose stiffness does not depend on the longitudinal or lateral directions (at high frequency, the longitudinal f_{11} and lateral f_{22} creepages coincide).

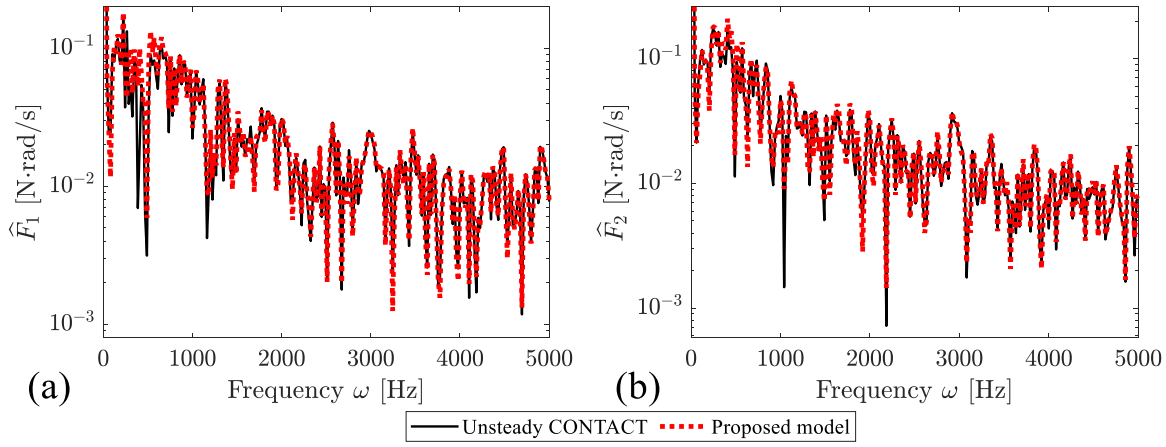

Fig. 9. Fourier transform of the contact force responses when $\bar{\xi}_1 = \bar{\xi}_2 = 0.0025$ and $\bar{\xi}_{sp} = -0.1$ rad/m, $\tilde{\xi}_1 = \tilde{\xi}_2 = 10^{-6}$ and $\tilde{\xi}_{sp} = 5{\cdot}10^{-6}$ rad/m for a pseudo-random creepage variation. Comparison between the results obtained by the unsteady CONTACT and those from the proposed model: (a) longitudinal force; (b) lateral force.

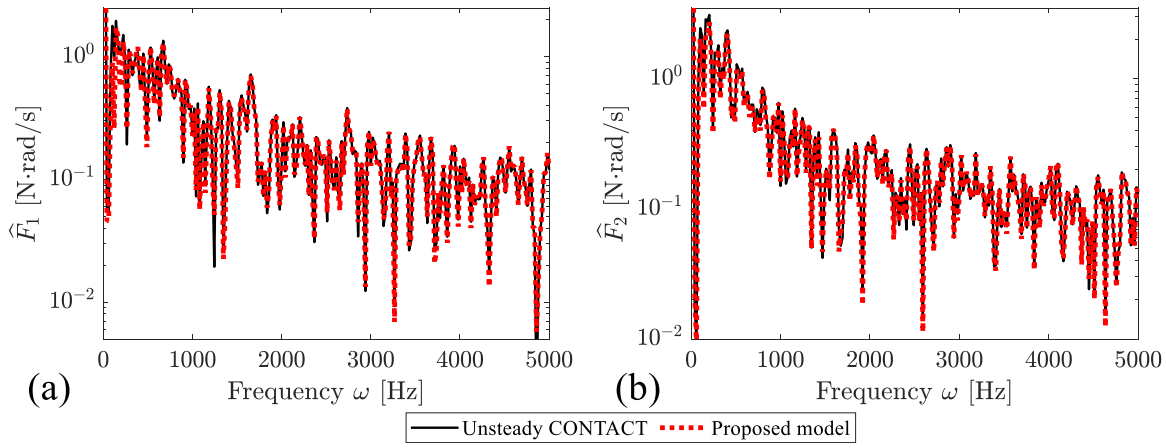

Fig. 10. Fourier transform of the contact force responses when $\bar{\xi}_1 = \bar{\xi}_2 = 0.001$ and $\bar{\xi}_{sp} = -0.053$ rad/m, $\tilde{\xi}_1 = \tilde{\xi}_2 = 10^{-5}$ and $\tilde{\xi}_{sp} = 5{\cdot}10^{-5}$ rad/m for a pseudo-random creepage variation. Comparison between the results obtained by the unsteady CONTACT and those from the proposed model: (a) longitudinal force; (b) lateral force.

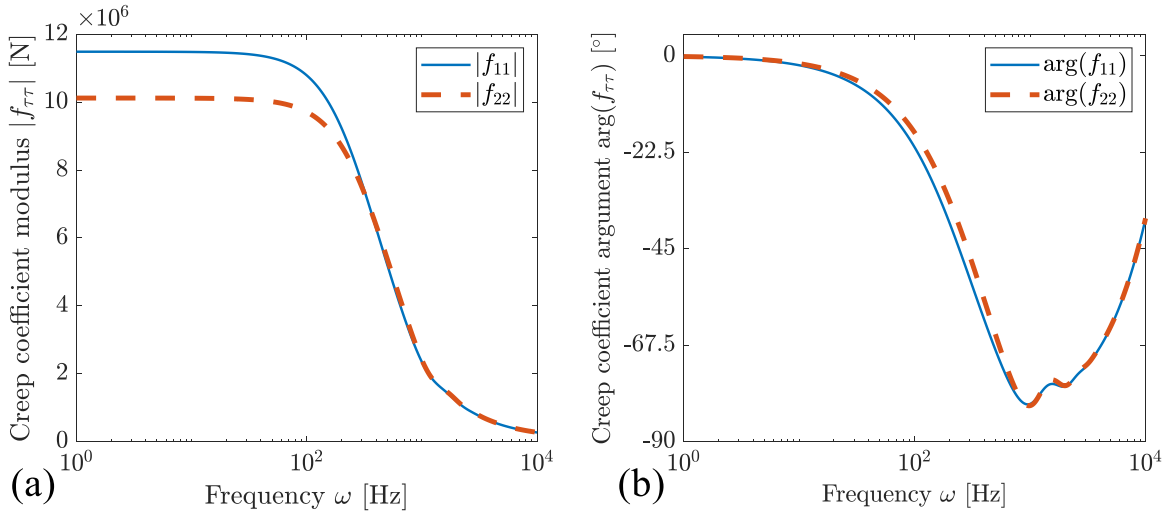

Fig. 11. Longitudinal f_{11} and lateral f_{22} creep coefficients as a function of frequency ω when $\bar{\xi}_1 = \bar{\xi}_2 = 0.001$ and $\bar{\xi}_{sp} = -0.053$ rad/m: (a) creep coefficient modulus; (b) creep coefficient argument.

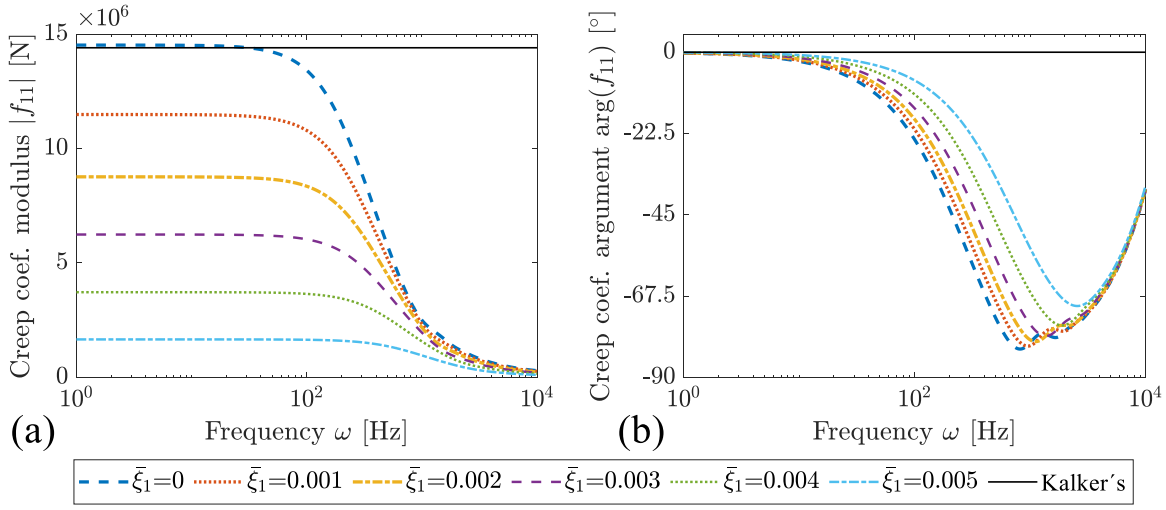

Fig. 12. Longitudinal f_{11} creep coefficient as a function of frequency ω for different mean longitudinal creepages. The plot also shows the creep coefficient calculated through Kalker's Linear Theory: (a) creep coefficient modulus; (b) creep coefficient argument.

Fig. 12 shows the longitudinal f_{11} creep coefficient calculated as a function of the creepage variation frequency ω for different mean longitudinal creepages $\bar{\xi}_1$. The mean lateral creepage $\bar{\xi}_2$ and the mean spin $\bar{\xi}_{sp}$ are zero. Fig. 12(a) presents the module of the creep coefficient, and Fig. 12(b) shows the argument. When comparing the creepages calculated using Kalker's Linear Theory and the proposed model for $\bar{\xi}_1 = 0$, there is a discrepancy between results at low frequency smaller than 1%. This is because the entire contact area is in adhesion when $\bar{\xi}_1 = 0$, producing infinite tractions at the trailing edge of the contact area. The proposed model cannot accurately reproduce this case, so it provides a higher creepage coefficient and, hence, the contact dynamic stiffness is higher. As the mean creepage increases, the adhesion area decreases, and the module of the creep coefficient with it, which confirms that the creep coefficient magnitude depends on the size of the adhesion area. Regarding the creep coefficient argument, a trend similar to that shown in Fig. 3 is observed.

3.5. Non-Hertzian case

This section analyses a problem in which the undeformed geometries of the solids in contact do not satisfy Hertz's hypotheses. The case corresponds to a wheelset with S1002 profiles centred on a track with UIC60 rails. The wheelset vertical load is 20 tons. In this case, the contact patch is not an ellipse, nor is the normal traction elliptical.

In this calculation, the mean creepage values adopted are $\bar{\xi}_1 = \bar{\xi}_2 = 0.001$ and $\bar{\xi}_{sp} = -0.053$ rad/m. Fig. 13 shows the mean tangential traction distribution for this case obtained through Eq. (3) (steady-state CONTACT). In this plot, the adhesion and slip areas are also differentiated through the arrow colours (blue-adhesion, red-slip) and using dots (that indicate the sliding elements).

The proposed method is applied to this non-Hertzian case in the same way it has been done in the previous examples. The creepages vary again according to a finite-bandwidth white-noise signal approached through Eq. (32). In this equation, 1000 frequencies uniformly distributed between 100 Hz and 1 kHz are implemented, and the harmonic amplitudes are $\tilde{\xi}_j = 10^{-6}$ for longitudinal and lateral creepages, and $\tilde{\xi}_{sp} = 5{\cdot}10^{-6}$ rad/m for the spin. The tangential forces calculated using the unsteady CONTACT model and the proposed one are compared in Fig. 14. The initial conditions imposed on the unsteady CONTACT model give rise to a short transient of approximately 0.001 s. After the transient, the

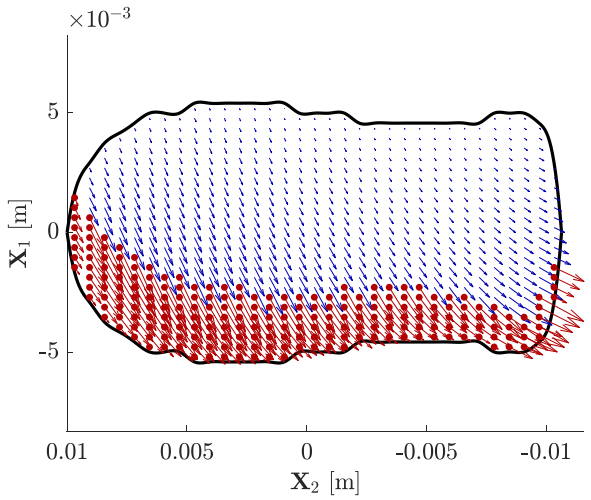

Fig. 13. Tangential traction distribution calculated through the steady-state CONTACT for $\bar{\xi}_1 = \bar{\xi}_2 = 0.001$ and $\bar{\xi}_{sp} = -0.053$ rad/m. Blue arrows are in the adhesion area whereas the slip area plots red arrows and dots. The rail and wheel profiles are UIC60 and S1002, respectively.

agreement of the proposed model and CONTACT is satisfactory. This result can also be analysed in the frequency domain through the spectra shown in Fig. 15. A proper fit is observed at all frequencies except in some dips that have a negligible influence on the response since the ordinate axis is in logarithmic scale.

4. Conclusions

The present work develops a new linear rolling-contact theory to solve the non-steady-state tangential problem in non-Hertzian contact areas. The proposed method requires the creepage to be decomposed into the sum of a constant mean term and a variable one, and it assumes that the slip and the adhesion areas do not change with time. The problem associated with the mean creepage term is solved by means of the steady-state version of CONTACT, using its results as input parameters of the new model. This theory is developed starting from the non-steady CONTACT equation which is approximated to a linear relationship between the variable term of the creepage and the contact traction distribution (or the corresponding resultant forces). According to this formulation, the non-steady state contact problem can be solved for any shape of the wheel/rail contact region with a much smaller computational effort than the one required by the general unsteady CONTACT approach. The results show a satisfactory agreement when comparing the proposed model and the unsteady CONTACT version, hence

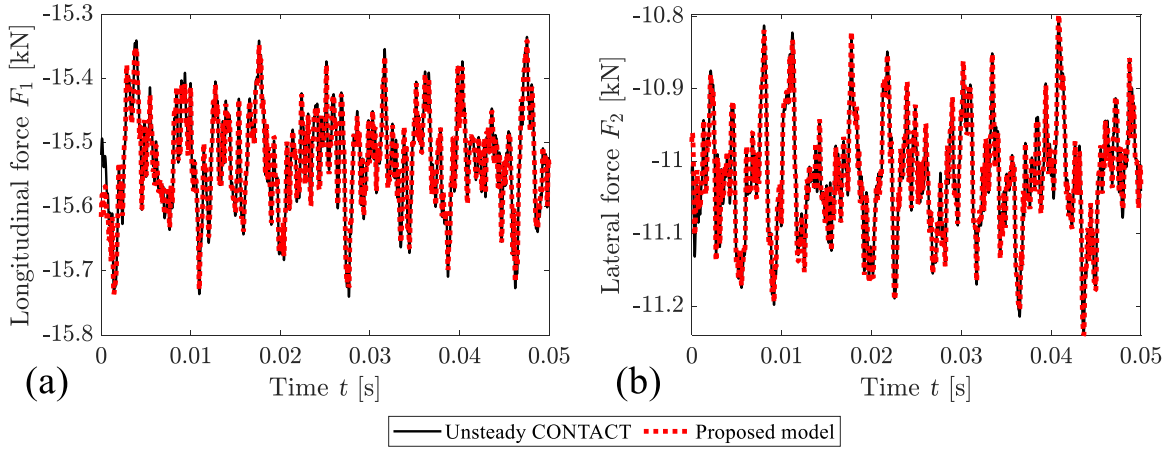

Fig. 14. Contact force responses to a pseudo-random creepage variation when $\bar{\xi}_1 = \bar{\xi}_2 = 0.001$, $\bar{\xi}_{sp} = -0.053$ rad/m, $\tilde{\xi}_1 = \tilde{\xi}_2 = 10^{-6}$ and $\tilde{\xi}_{sp} = 5{\cdot}10^{-6}$ rad/m. Comparison between the results obtained by the unsteady CONTACT and those from the proposed model for a non-Hertzian area: (a) longitudinal force; (b) lateral force.

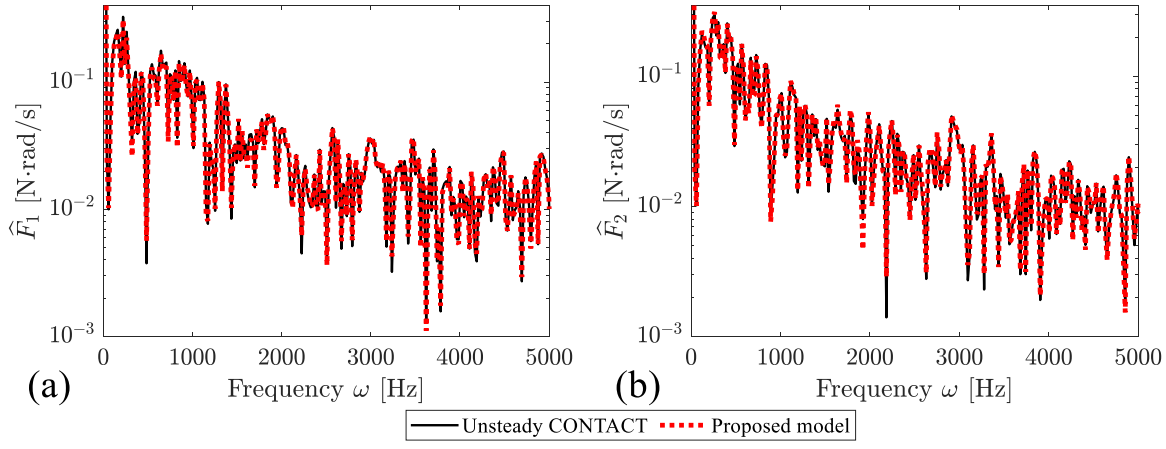

Fig. 15. Fourier transform of the contact forces presented in Fig. 14. Comparison between the results obtained by unsteady CONTACT and those from the proposed model for a non-Hertzian area: (a) longitudinal force; (b) lateral force.

confirming the soundness of the proposed contact model.

Creep coefficients computed through this method depend on the mean creepage level and the variable creepage frequency. This implies that the contact capability to dissipate energy decreases when the mean creepage and the frequency increase, hence the contact acts as a stiffness between the wheel and the rail in certain frequency bands.

The new theory allows the calculation of the interaction between a railway vehicle and the track through a linear model for cases with non-negligible mean creepage levels added to a variable component at medium/high frequency. This condition occurs when the vehicle passes through a curve (in which the mean creepage is due to the steering forces and the variable creepage from the coupled vehicle-track vibration), during braking or running-in. The new formulation will also help open the door to calculations in the frequency domain (e.g. rolling noise) associated with vehicles running on a curve, and to the analysis of squeal and corrugation in curves through linearised models.

Declaration of Competing Interest

The authors declare that they have no known competing financial interests or personal relationships that could have appeared to influence the work reported in this paper.

Data Availability

No data was used for the research described in the article.

Acknowledgments

The first and third authors acknowledge the financial support through the grants PID2020-118013RB-C21 (funded by MCIN/AEI/10.13039/501100011033) and PROMETEO/2021/046 (funded by Generalitat Valenciana).

Statement of originality

This is to certify that to the authors' knowledge, the content of this article is our own work. The authors of the present article certify that this paper is our original unpublished work and it has not been submitted to any other journal for reviews.

References

[1] Lewis R, Olofsson U, editors. Wheel/rail interface handbook. Woodhead publishing; 2009.
[2] Meymand SZ, Keylin A, Ahmadian M. A survey of wheel–rail contact models for rail vehicles. Veh Syst Dyn 2016;54(3):386–428.
[3] Vollebregt E, Six K, Polach O. Challenges and progress in the understanding and modelling of the wheel–rail creep forces. Veh Syst Dyn 2021;59(7):1026–68.
[4] Thompson DJ. Railway noise and vibration: mechanisms. Modelling and Means of Control. Oxford, UK: Elsevier; 2009.
[5] Kalker JJ. A minimum principle for the law of dry friction. Part 2: Application to nonsteady rolling elastic cylinders. J Appl Mech 1971;38:881–7.
[6] Kalker JJ. Three dimensional elastic bodies in rolling contact. Dordrecht/Boston/London: Kluwer Academic Publishers; 1990.
[7] E.A. H. Vollebregt, "New insights in non-steady rolling contact," in Proceedings of the 24th International Symposium on Dynamics of Vehicles on Roads and Tracks, 2015, pp. 1–4.
[8] Vila P, Baeza L, Martínez-Casas J, Carballeira J. Rail corrugation growth accounting for the flexibility and rotation of the wheel set and the non-Hertzian and non-steady-state effects at contact patch. Veh Syst Dyn 2014;52(SUPPL. 1):92–108.
[9] Johnson KL. Contact mechanics. Cambridge: Cambridge University Press; 1985.
[10] Vollebregt E. A new solver for the elastic normal contact problem using conjugate gradients, deflation, and an FFT-based preconditioner. J Comput Phys 2014;257(Part A):333–51.
[11] Zhao J, Vollebregt E, Osterlee C. A fast nonlinear conjugate gradient based method for 3D concentrated frictional contact problems. J Comput Phys 2015;288:86–100.
[12] Shen Z, Li Z. A fast non-steady state creep force model based on the simplified theory. Wear 1996;191(1–2):242–4.
[13] Alonso A, Giménez JG. Non-steady state modelling of wheel-rail contact problem for the dynamic simulation of railway vehicles. Veh Syst Dyn 2008;46(3):179–96.
[14] Guiral A, Alonso A, Baeza L, Giménez JG. Non-steady state modelling of wheel–rail contact problem. Veh Syst Dyn 2013;51(1):91–108.
[15] Knothe K, Gross-Thebing A. Derivation of frequency dependent creep coefficients based on an elastic half-space model. Veh Syst Dyn 1986;15(3):133–53.
[16] Gross-Thebing A. Frequency-dependent creep coefficients for three-dimensional rolling contact problems. Veh Syst Dyn 1989;18(6):359–74.
[17] Blanco-Lorenzo J, Santamaria J, Vadillo EG, Correa N. On the influence of conformity on wheel–rail rolling contact mechanics. Tribology Int 2016;103:647–67.
[18] Liu B, Fu B, Bruni S. Generalisation of the linear theory of rolling contact to a single double-elliptic contact region and its application to solve non-Hertzian contact problems using extended FASTSIM. Veh Syst Dyn 2022:1–19.